Precision targeting of liver lesions using a novel electromagnetic navigation device in physiologic phantom and swine

Filip Banovac[a)] and Jonathan Tang
Imaging Sciences and Information Systems Center, Department of Radiology, Georgetown University, Washington, DC 20007

Sheng Xu
Center for Computer Integrated Surgical Systems and Technology, Johns Hopkins University, Baltimore, Maryland 21211

David Lindisch and Ho Young Chung
Imaging Sciences and Information Systems Center, Department of Radiology, Georgetown University, Washington, DC 20007

Elliot B. Levy, Thomas Chang, and Michael F. McCullough
Georgetown University Hospital, Washington, DC 20007

Ziv Yaniv
Imaging Sciences and Information Systems Center, Department of Radiology, Georgetown University, Washington, DC 20007

Bradford J. Wood
Special Procedures DRD, National Institutes of Health, Bethesda, Maryland 20892

Kevin Cleary
Imaging Sciences and Information Systems Center, Department of Radiology, Georgetown University, Washington, DC 20007

(Received 17 November 2004; revised 26 April 2005; accepted for publication 8 June 2005; published 29 July 2005)

Radiofrequency ablation of primary and metastatic liver tumors is becoming a potential alternative to surgical resection. We propose a novel system that uses real-time electromagnetic position sensing of the needle tip to help with precision guidance into a liver tumor. The purpose of this study was to evaluate this technology in phantom and animal models. Using an electromagnetic navigation device, instrumented 18 g needles were advanced into radioopaque tumor targets in a respiratory liver phantom. The phantom featured a moving liver target that simulated cranio-caudal liver motion due to respiration. Skin-to-target path planning and real-time needle guidance were provided by a custom-designed software interface based on pre-operative 1 mm CT data slices. Needle probes were advanced using only the electromagnetic navigation device and software display. No conventional real-time imaging was used to assist in advancing the needle to the target. Two experienced operators (interventional radiologists) and two inexperienced ones (residents) used the system. The same protocol was then also used in two anesthetized 45 kg Yorkshire swine where radioopaque agar nodules were injected into the liver to serve as targets. A total of 76 tumor targeting attempts were performed in the liver phantom, and 32 attempts were done in the swine. The average time for path planning was 30 s in the phantom, and 63 s in the swine. The median time for the actual needle puncture to reach the desired target was 33 s in the phantom, and 42 s in the swine. The average registration error between the CT coordinate system and electromagnetic coordinate system was 1.4 mm (SD 0.3 mm) in the phantom, and 1.9 mm (SD 0.4 mm) in the swine. The median distance from the final needle tip position to the center of the tumor was 6.4 mm (SD 3.3 mm, $n=76$) in the phantom, and 8.3 mm (SD 3.7 mm, $n=32$) in the swine. There was no statistical difference in the planning time, procedure time, or accuracy of needle placement between experienced and inexperienced operators. The novel electromagnetic navigation system allows probe delivery into hepatic tumors of a physiologic phantom and live anesthetized swine. The system allows less experienced operators to perform equally well as experienced radiologists in terms of procedure time and accuracy of needle probe delivery. © *2005 American Association of Physicists in Medicine*. [DOI: 10.1118/1.1992267]

Key words: electromagnetic navigation, instrument tracking, radiofrequency ablation, liver tumor

I. INTRODUCTION

Radiofrequency (RF) ablation of hepatic tumors is becoming a potential alternative to surgical resection or cryotherapy. Several prospective trials have established the efficacy and safety of RF ablation, both by percutaneous methods[1] and intra-operatively,[2] in the treatment of hepatocellular carci-

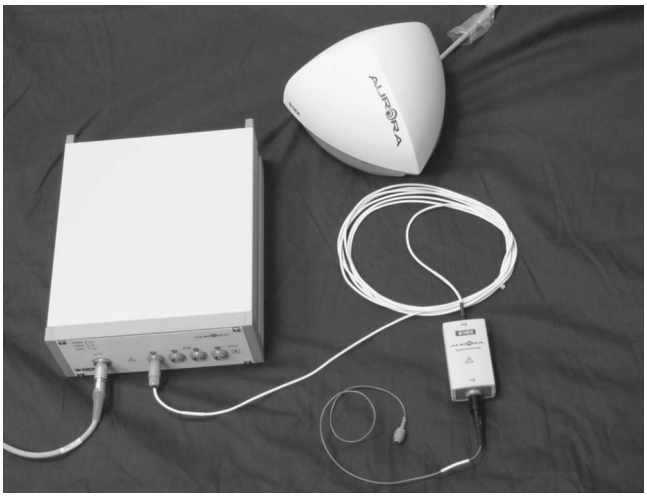

FIG. 1. Electromagnetic navigation device consists of a field generator (top), a control unit (left), and a sensor interface device (bottom right). The interface device allows attachment of various tracked instruments which can be localized in the electromagnetic coordinate system in front of the faceplate of the field generator.

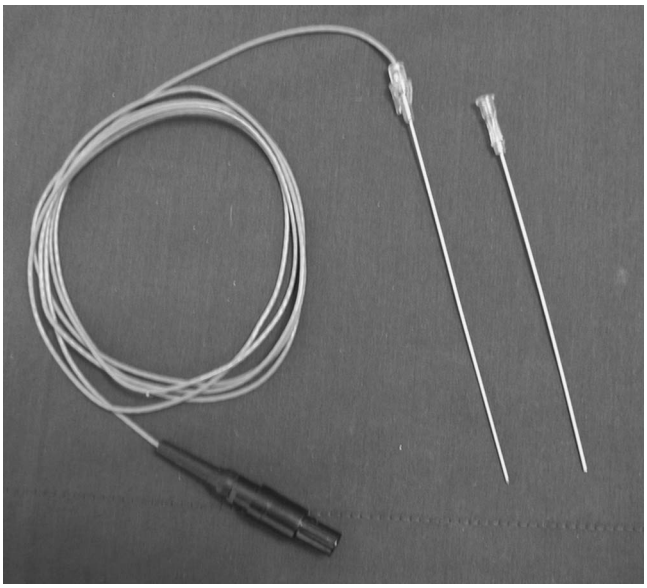

FIG. 2. Two needles with a coil in the tip (coil not seen). Needles can be attached to the interface device of the electromagnetic navigation system. This allows for real time tracking of the needle tip in the electromagnetic coordinate system.

noma (HCC) and liver metastases, and especially for unresectable tumors.[3] Two large studies report that RF ablation without resection or cryotherapy has a disease-free survival rate of 70% at 12–15 months.[1,4] The cost effectiveness of RF therapy has also been demonstrated.[5]

One of the main challenges for improving RF ablation is to position the needle more precisely within the tumor to achieve adequate treatment margins. Ultrasound, and to a lesser extent CT, have been used as primary modalities in RF probe placement, each with their own advantages and limitations. Electromagnetic navigation and guidance of needles or medical instruments has been shown in a variety of applications. Solomon *et al.* demonstrated at least three separate medical procedures, significantly different from one another, where electromagnetic guidance of instruments was used to achieve a desired clinical goal. They used the technology in creation of a transjugular intrahepatic portosystemic shunt creation,[6] bronchoscopic navigation,[7] and in deployment of a vena cava filter.[8] More recently, electromagnetic navigation has been used in clinical series with applications in radiofrequency ablation of conductive pathways in the heart.[9]

We developed and tested a novel electromagnetic navigation system in an attempt to improve the accuracy of probe placement when used alone or as an adjunct to present guidance modalities. The new system uses an electromagnetic field sensing device that can track the position of small sensors embedded in needles or instruments. By integrating this navigation system with pre-procedural CT imaging, we tested the concept in one phantom and two swine.

II. MATERIALS AND METHODS

A. Electromagnetic navigation system

We used a commercially available electromagnetic localizer AURORA (Northern Digital Inc., Waterloo, Ontario, Canada), which consists of a field generator, a control unit, and a sensor interface device (Fig. 1). This system was integrated with an 18-gauge MagTrax Needle (Fig. 2) (Traxtal, Bellaire, TX), which contains a miniature sensor coil (Fig. 3) in the tip of the needle. This sensor allows the AURORA to localize the needle tip and return the position of the needle tip in the coordinate space. Subsequent registration with preoperative CT images was carried out using a respiratory liver phantom[10] and two 45 kg Yorkshire swine.

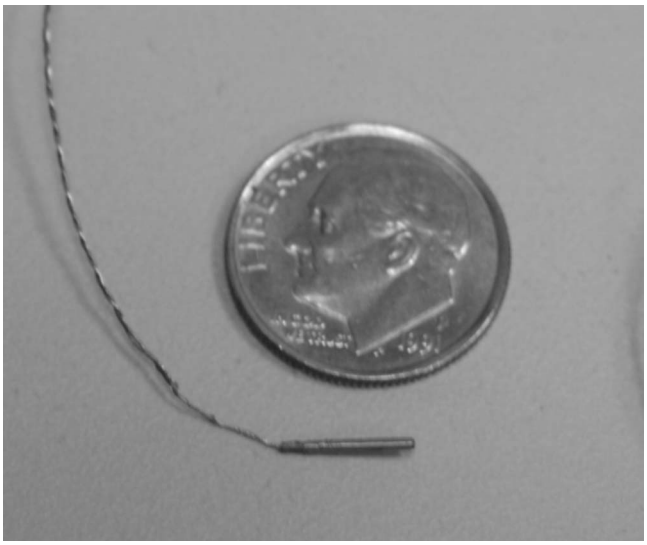

FIG. 3. A prototype coil with wire connectors (bottom) is small 8 mm by 0.8 mm, allowing incorporation into other medical instruments such as needles, trocars, and catheters.

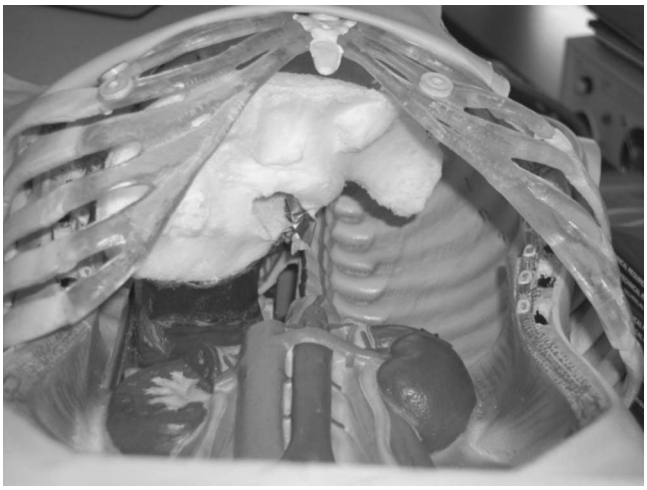

FIG. 4. A foam liver model (middle) is amenable to needle puncture. It is mounted on the single axis of motion platform inside a model torso. The platform can oscillate in cranio-caudal direction and simulate the motion of the liver seen in physiologic respiration.

B. Respiratory liver phantom and motion control software

We developed a liver respiratory motion simulator,[10] consisting of a torso and a custom foam liver model mounted on a single axis moving platform (Fig. 4). The liver is amenable to needle puncture and contains radio-opaque foam tumors. A liver phantom was created using a custom-designed mold. Flex Foam-iT III (Smooth-On Inc., Easton, PA) was cured in the liver mold. Two spherical targets (1 to 2 cm diameter), also made out of FlexFoam-iT III, were cured after addition of dilute CT contrast and inserted into the foam liver to serve as needle targets. The foam liver was mounted onto a motor control unit which allowed for simulation of liver movement during respiration. Variable respiratory rates and patterns could be simulated.

C. Animal preparation

Animal use for the experiments was approved by the Division of Comparative Medicine (DCM) veterinary staff. They anesthetized and endotracheally intubated each swine. Using a modification of the technique described by Tsuchida *et al.*, 1 to 2 ml of purified agar dissolved in distilled water and diluted in CT contrast medium (1:10 v/v dilution) was percutaneously injected into the swine liver using an 18 g needle.[11] Two agar injections were performed for each animal to serve as nodular targets approximately 1 to 2 cm in diameter. The animals were pharmacologically paralyzed using pancuronium 0.1–0.2 mg/kg. Ventilatory support and continuous monitoring of vital signs were done by the DCM veterinary staff. While holding respiration in expiratory phase, pre-procedural CT scans of each animal were performed. The swine were then transferred to the angiography suite for the nodule targeting experiments.

FIG. 5. A radiology resident is using the electromagnetic navigation system to guide the needle into the nodular target using the GUI. A typical puncture starts with path planning followed by needle puncture algorithm which displays a graphical representation of the needle on the GUI in real time.

D. CT imaging and registration

Pre-procedural CT imaging, first for the phantoms and later for the swine, was carried out on the Volume Zoom Multi-detector CT Scanner (Siemens, Erlangen, Germany. Volumetric acquisition with 1 mm slice thickness from the top of the liver through the caudal aspect of the liver was obtained for each subject. In each case, four Multi-Modality Fiducial Markers (IZI Medical, Baltimore, MD) were placed on the skin, and one active MagTrax needle fiducial was placed into liver parenchyma before the scan. Scanning was performed during the full expiratory phase of the respiratory cycle in both the phantom and the swine. In the phantom, the expiratory position of the liver was considered the location with the most cranial displacement of motion. In the swine, the veterinary specialist suspended respiration of the animal in full expiration while the CT scan was obtained.

The position of each skin fiducial marker was obtained during the registration process by touching each fiducial with an electromagnetically tracked MagTrax Probe (Traxtal Inc., Bellaire, TX) and recording the position in the electromagnetic coordinate system. Corresponding fiducials were then selected on the CT slices by scrolling to the appropriate slice and selecting the correct fiducial with a mouse. Transformation between the two coordinate systems was then performed by using a least square method[12] to determine the rigid-body transformation between the CT coordinate system and the AURORA coordinate system.

E. Procedure planning and image navigation software

A graphical user interface named IGBiopsy, originally used for electromagnetically assisted biopsy, has been developed by our group.[13] The software interfaced to the electromagnetic navigation system and allowed for simultaneous display of an electromagnetically tracked instrument and the corresponding CT slices. The orientation and position of the instrument relative to the simulator or the animal determined the slice position and multiplanar slice reconstruction. The system allowed the user to plan the needle positioning on

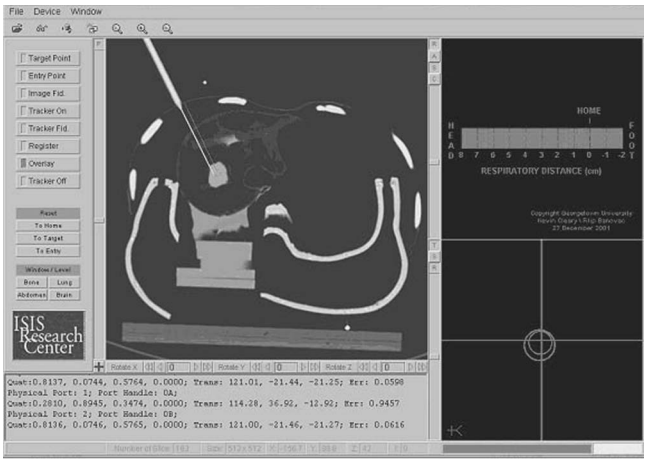

FIG. 6. A an off-axial cross sectional image of the phantom liver is seen as the needle approaches the tumor (center left). A depth of insertion window (top right) allows the user to insert the needle to the appropriate depth based on pre-procedural planning and registration. A cross-hairs targeting window (bottom right) allows the user to keep the needle in correct orientation during the puncture; the smaller circle in the middle of the cross hairs corresponds to the location of the needle tip. It has to be included in its entirety within the outer circle, which depicts the location of the hub of the needle, in order to stay on the correct path to the target.

previously acquired CT images, and thus helped guide the needle to the exact location within the tumor (Fig. 5). First, the physician selected the appropriate skin entry point on the IGBiopsy graphical user interface (GUI). Second, an appropriate path to the nodular target was selected, followed by the registration process as described above.

Our software visualization included a display in axial, sagittal, and off-axial planes. Here, the needle instrument was displayed in real time on the pre-acquired CT images. Additionally, a cross-hairs targeting window displayed the trajectory of the needle tip to the target in real time, thus allowing for small adjustments in puncture trajectory and depth of insertion (Fig. 6).

F. Targeting experiments

Two experienced interventional radiologists and two radiology residents participated in the study. Seventy-six targeting passes into a target nodule were performed in liver phantoms on two separate days (36 on first day and 40 on the second day), and 32 targeting passes into a nodule were made in two swine (16 passes into each animal). The duration of each step—of the procedure planning, needle manipulation, and procedure itself—was recorded for each physician. On each day of experimentation, registration was initially performed prior to the first set of punctures. After 10–12 passes, registration was repeated to avoid error caused by slight motion of the animals or slight displacement of the phantom.

Registration and actual needle punctures were performed while the phantom was in the full expiratory phase of the respiratory cycle. Likewise, registration and needle manipulation was also performed while the animal was in full expiration. This was done by allowing a fully anesthetized and pharmacologically paralyzed animal to exhale for 30–35 s while the needle was advanced. Using this methodology, we tried to replicate liver position obtained during CT scanning and minimize the error due to the movement of target between registration and implantation.

Each physician advanced the needle towards the nodule in the phantom or swine using only the GUI; no real time imaging equipment was used. Once the physician was satisfied that the needle tip was in the desired final location, the needle pass was considered complete and respective times were recorded. Needle position was then verified with fluoroscopic imaging in anteroposterior and lateral (orthogonal) views, and images were captured for off-line analysis. Root mean square distances, from the final needle tip position to the center of the nodule, were calculated.

The root mean square (RMS) distance for the phantom experiments was calculated as

$$\mathrm{RMS} = \sqrt{(\mathrm{AP}_1 - \mathrm{AP}_0)^2 + (\mathrm{LAT}_1 - \mathrm{LAT}_0)^2}, \quad (1)$$

where AP_1 is the final needle tip position in the anterior-posterior (AP) plane, AP_0 is the position of the center of the tumor target in the AP plane, LAT_1 is the final needle tip position in the lateral plane, and LAT_0 is the position of the center of the tumor target in the lateral fluoroscopic plane. It should be noted that this formula is conservative in that it over-estimates the error since one dimension appears in both the AP and lateral plane. For the swine experiments, we broke out the components separately to more accurately compute the distance errors.

Therefore, for the swine experiments, the root mean square distance was computed as

$$\mathrm{RMS} = \sqrt{(X_1A - X_0A)^2 + (Y_1A - Y_0A)^2 + (Z_1L - Z_0L)^2} \quad (2)$$

Here, $X_1A - X_0A$ is the X component difference of the final needle position from the center of tumor in the AP plane; $Y_1A - Y_0A$ is the Y component difference of the final needle position from the center of tumor in the AP plane; and $Z_1L - Z_0L$ is the Z component difference of the final needle position from the center of tumor in the lateral plane.

Using the same planned path, the second physician would try to target the lesion. After each physician made one targeting attempt, a new path was chosen and the process was repeated. The path planning step of the procedure was alternated between the attending and the resident physician in order to eliminate any error introduced by inexperience in appropriate path planning.

G. Registration error

The registration between the anatomy and the CT scan was computed after each set of targeting passes (range 10–12 needle passes). For each registration attempt, the fiducial registration error (FRE) was calculated using the method described in Fitzpatrick[14] as follows:

$$\mathrm{FRE}^2 \equiv \frac{1}{N}\sum_{i=1}^{N} |\mathbf{R}x_i + \mathbf{t} - y_i|^2 \quad (3)$$

where:

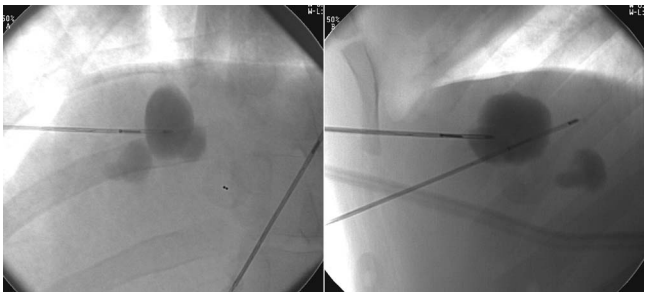

FIG. 7. Anteroposterior (left) and lateral (right) fluoroscopic images of a needle after it was inserted into the radio-opaque tumor target. Fluoroscopy was used to measure the distance of the needle tip from the center of the radio-opaque tumor only after the puncture was already completed using the electromagnetic navigation device. The second needle seen in the images represents the internal fiducial used for registration.

N is the number of fiducials
x_i is the position of the ith fiducial in the CT image
R is the rotation matrix of the transformation
t is the translation vector of the transformation
y_i is the position of the ith fiducial in the electromagnetic coordinate system

H. Statistical analysis

Two practice attempts were allowed in the beginning of each experimental series to allow for a learning curve with the software, needles, phantoms, and animal anatomy. These were not included in the reported data or in the statistical analysis.

Experiments were designed to evaluate the differences in performance between experienced and inexperienced operators. The Students' paired t-test was used to evaluate the differences in planning time, procedure time, and accuracy of needle targeting between the interventional radiologists and inexperienced radiology residents.

To evaluate for presence of consistent directional bias in our targeting attempts, error measurements were assessed for each of the X, Y, and Z coordinates. The distribution of the measurement errors were assessed for normality. Each of the error measurements were normally distributed and one sample t-tests were used to test if the mean error measurements were different from a hypothesized mean of 0 for each of the X, Y, and Z coordinates. If the error measurement were random, the 95% confidence interval around the mean measurement error would contain 0.

III. RESULTS

Seventy-six tumor targeting attempts were performed in the liver phantom, and 32 attempts were made in the swine. The average time for path planning was 30 s in the phantom and 63 s in the swine. The average time for the actual needle puncture to reach the desired target was 33 s in the phantom and 42 s in the swine.

The median distance from the final needle tip position to the center of the tumor was 6.4 mm (SD 3.3 mm, $n=76$) in the phantom and 8.3 mm (SD 3.7 mm, $n=32$) in the swine.

TABLE I. Times of needle puncture, and final distances to the center of the tumor target (mm) in swine livers. Comparison between experienced interventional radiologist and inexperienced radiology resident.

	Needle puncture time (s)		Distance from center of target (mm)	
Pass Number	Attending Radiologist	Resident Radiologist	Attending Radiologist	Resident Radiologist
1	51	45	8.9	10.7
2	16	27	13.6	7.2
3	125	90	11.4	9.9
4	40	48	13.8	9.6
5	33	33	2.9	7.1
6	33	42	8.2	4.9
7	40	38	11.0	9.4
8	35	42	9.6	4.1
9	42	44	8.3	6.7
10	40	45	11.3	10.8
11	45	53	18.0	3.7
12	33	43	3.3	12.4
13	33	45	5.8	7.3
14	35	58	10.1	4.5
15	37	50	4.2	7.3
16	41	41	3.3	3.1

Figure 7 shows typical fluoroscopic images in anteroposterior and lateral planes from the final needle position of a puncture in the swine.

The average registration error between the CT coordinate system and electromagnetic coordinate system was 1.4 mm (SD 0.3 mm) in the phantom and 1.9 mm (SD 0.4 mm) in the swine.

Each approach to the target was attempted by both the experienced interventional radiologist and an inexperienced resident. Results in the swine experiments are summarized in Table I.

The largest miss of the target nodule in swine was 1.2 cm for the resident and 1.8 cm for the attending interventional radiologist.

Table II compares the outcomes between the physicians.

There was no statistically significant difference in the planning time, procedure time, or accuracy of needle placement between experienced and inexperienced operators.

A bias analysis of the swine data was performed to examine whether there was any consistent directional error during needle insertion. Table III summarizes the mean error values along component coordinates for all 32 targeting attempts in swine.

Taken individually, the mean values represent the estimated bias in the respective coordinate direction. Taken together, these coordinates provide the center-point of the 32 measurements made in three-dimensions. The direction of bias is given by the vector associated with the center point $(-1.03, 2.83, -0.41)$ indicating a positive drift in the Y direction, with a slight negative deflection in X and minimal negative deflection in Z. A statistical test of the overall bias can be

TABLE II. Comparison of path planning time, needle puncture time, and average distance of each needle puncture from the center of the desired target.

	Mean path planning time (s)±SD		Median needle puncture time (s)±SD		Median distance from center of tumor (mm)±SD	
	Attending	Resident	Attending	Resident	Attending	Resident
Respiratory Phantom (n=76)	30±10	29±14	28±23	38±32	6.4±3.2	6.4±3.3
	p=0.76		p=0.14		p=0.99	
Swine (n=32)	63±43	64±17	39±23	44±14	9.2±4.3	7.2±2.8
	p=0.94		p=0.55		p=0.25	

calculated and is significant ($p<0.007$), but this can be attributed to the large error observed in the Y coordinate.

Additionally, when analyzed independently, a statistically significant drift along the Y axis for both resident ($p<0.02$) and attending ($p<0.05$) physician was present. However, there was no statistically significant inter-operator difference along any of axis.

Table IV summarizes the total number of successful and unsuccessful targeting attempts for each level of operator experience.

IV. DISCUSSION

Although RF ablation is becoming a commonly used modality in the primary treatment of HCC and liver metastases, the procedure has several technical limitations which are mostly related to the difficulty of precisely positioning the needle to ablate the entire tumor and achieve adequate margins. Recurrence of disease has been associated with tumor size and thus with the total volume of tumor ablated, the largest tumors having the highest recurrence rates.[15] Inadequate volumetric coverage of tumors during a single needle insertion necessitates several probe repositionings during the procedure.[15,16] These adjustments are essential to obtain adequate treatment margins, but can be technically difficult.

Positioning the probe in multiple locations within the tumor to achieve overlapping spheres of treatment is difficult because geometric overlap of treatment spheres is hard to visualize. Using an early version of RF technology (a single electrode rather than the multipronged devices now available), Dodd *et al.* indicated that, on the basis of a 3 cm thermal injury, tumors that are larger than 3 cm can require up to 12 overlapping ablations to treat the tumor volume with adequate margins.[17] The resultant area of combined spherical treatments does not correspond to the larger, usually spherical tumor.[15] Therefore, the ablation of most tumors requires multiple probe placements, making the precise placement of the probe highly desirable.[18] Additionally, the tumor often recurs in a circular fashion around the original tumor and is hard to treat with follow-up applications of RF,[19] as repeat treatment is geometrically unfavorable.

Therefore, a guidance system such as ours could improve the treatment of liver tumors and metastases. Granted, our system has its limitations: Namely, the median distance of needle placement from the desired center of the targets is still too large (6.4 mm in phantom and 8.3 mm in swine). In a clinical setting such errors could result in ablation of tissue other than the tumor, or worse, ablation of other critical structures in the vicinity of the tumor. Therefore, the system must be improved.

This study did not evaluate the possible sources of error in needle placement; however, some of them are evident. Registration error is a function of the overall accuracy of the electromagnetic navigation system, and is compounded by the methodology we used in imaging and fiducial selection. In this study, we treated the liver in the swine as a rigid body for purposes of registration, which it clearly is not. Surface fiducials also move with respiration as the chest wall expands and retracts. In fact, respiratory motion *per se* introduces an error that should be quantified in a future study. A more detailed evaluation of respiratory motion as a source of error should be performed prior to clinical utilization of the electromagnetic navigation system.

We tried to minimize the error introduced by respiratory motion by obtaining the pre-procedural CT scan in full expiration, and performing our registration in the angiography suite in full expiration as well. However, one has to account for the transportation of the animal from the CT scanner to the angiography suite; any motion or change in the animal's position could have been another source of registration error.

TABLE III. Mean error values along component coordinates in swine studies.

Coordinate	Mean±SD	95% CI	p value[a]
Total X	−1.03±5.67	−3.08, 1.01	0.31
Total Y	2.83±4.86	1.07, 4.58	0.003
Total Z	−0.41±4.22	−1.93, 1.12	0.59

[a]One sample t-test.

TABLE IV. Total number of successful (hits) and unsuccessful (misses) of the 1 to 2 cm tumor targets in phantom and swine for resident and attending radiologists.

	Operator			
	Resident Radiologist		Attending Radiologist	
	HIT	MISS	HIT	MISS
Phantom (n=76)	36	2	37	1
Swine (n=32)	10	6	10	6

We did not consider a detailed analysis of sources of error to be one of the main goals of this study, however this important topic using the same AURORA electromagnetic localizing system has already been published by Hummel and colleagues.[20] These authors evaluated the influence of surgical instruments and radiological equipment on the field distortion and resultant error of the system.

Our RMS error analysis for the phantom experiments and the swine experiments is slightly different as noted earlier. In fact, the RMS analysis in the phantom studies slightly overestimates the error. In Eq. (1) as we are inherently including the same component vector in the cranio-caudal axis of the phantom (Y axis of the fluoroscopic system) is included in measuring the distance in both the AP and the LAT planes. We therefore performed the swine experiments and error calculations by breaking our final needle displacements from the center of the tumor target into component vectors Eq. (2). This approach better estimates the true errors of the final needle position with respect to the tumor centers. Admittedly, one of the weaknesses of our study was our approach to calculating the error. We reported the FRE but not the target registration error (TRE) in this study. In our post-procedural analysis, we did not have sufficient CT data to calculate the TRE. We plan to remedy this in our future work.

Our directional error analysis (Table III) showed that there is bias in our experiments. It is not intuitive why we encounter a consistent drift in the Y coordinate. In physical space, based on the definition of our coordinate systems, this would suggest that we tend to deviate caudally (toward the feet). It is conceivable that we encountered a slight postural change of the animal along that component vector and that this was not recognized at the time of the experiments. This illustrates the importance of patient positioning in any future applications of this technology. In addition, dynamic referencing points or some other manual or semiautomatic methods of checking for these postural changes should be included in the system prior to any human trials. Additionally, correcting the consistent drift should improve the overall success rate in hitting the target (Table IV). Missing the target in 6 out of 16 attempts by each of the operators is not clinically acceptable. We believe that future improvements in our methodology will improve the accuracy and reduce the "miss" rate.

The time it takes to plan the procedure on the GUI and the time it takes to perform the needle puncture when using the system is in fact very promising. There was no statistical difference in the planning time or the needle puncture time when comparing experienced interventional radiologists to inexperienced resident physicians. Compared to clinical practices that use CT guidance or CT fluoroscopic guidance, in which radiofrequency probe insertion and deployment can take much longer, the median of 63 s for path planning and 42 s for needle puncture is an improvement. However, one must concede that the pre-procedural imaging, animal transportation between the CT and angiography suites, and registration used in our methodology all add time to the three steps outlined above. The overall procedure times of conventional RFA methods and our electromagnetic navigation system should be compared in a separate study.

Finally, our system overcomes some of the traditional limitations of other modalities used for image guidance into liver tumors. Namely, when using ultrasound to guide a probe into the liver, the hyperechogenicity of the ablated tissue that occurs during treatment can obscure the visualization of the deeper parts of the lesion and make repositioning technically difficult.[21] An intense hyperechoic sonographic pattern caused by gas bubble formation[18,19] can require 5–10 min after the end of the treatment to dissipate enough to visualize the needle repositioning. Moreover, precise needle tip position is often difficult to visualize with ultrasound.[22] When using the electromagnetic navigation system, such limitations are not an issue.

V. CONCLUSION

Our novel electromagnetic navigation system allowed probe delivery into hepatic tumors in a physiologic phantom and in live anesthetized swine. The system allowed less experienced operators to perform just as well as experienced radiologists in terms of procedure time and accuracy of needle probe delivery. The overall accuracy of the system remains a challenge and offers a topic for future work.

ACKNOWLEDGMENTS

This work was funded in part by Radiological Society of North America Holman Resident Seed Grant, and in part by U.S. Army Grant No. DAMD17-99-1-9022. The content of this manuscript does not necessarily reflect the position or policy of the U.S. Government. We would like to thank Dr. Michael Fitzpatrick for professional advice in preparing this manuscript.

[a]Author to whom correspondence should be addressed. Telephone: (202) 687-0054; Fax: (202) 784-4379. Electronic mail: banovac@isis.imac.georgetown.edu

[1]S. A. Curley, F. Izzo, P. Delrio, L. M. Ellis, J. Granchi, P. Vallone, F. Fiore, S. Pignata, B. Daniele, and F. Cremona, "Radiofrequency ablation of unresectable primary and metastatic hepatic malignancies: results in 123 patients," Ann. Surg. **230**(1), 1–8 (1999).

[2]A. J. Bilchik, D. M. Rose, D. P. Allegra, P. J. Bostick, E. Hsueh, and D. L. Morton, "Radiofrequency ablation: a minimally invasive technique with multiple applications," Cancer J. Sci. Am. **5**(6), 356–361 (1999).

[3]B. J. Bowles, J. Machi, W. M. Limm, R. Severino, A. J. Oishi, N. L. Furumoto, L. L. Wong, and R. H. Oishi, "Safety and efficacy of radiofrequency thermal ablation in advanced liver tumors," Arch. Surg. (Chicago) **136**(8), 864–869 (2001).

[4]A. Siperstein, A. Garland, K. Engle, S. Rogers, E. Berber, A. Foroutani, A. String, T. Ryan, and P. Ituarte, "Local recurrence after laparoscopic radiofrequency thermal ablation of hepatic tumors," Ann. Surg. Oncol. **7**(2), 106–113 (2000).

[5]S. K. Shetty, M. P. Rosen, V. Raptopoulos, and S. N. Goldberg, "Cost-effectiveness of percutaneous radiofrequency ablation for malignant hepatic neoplasms," J. Vasc. Interv Radiol. **12**(7), 823–833 (2001).

[6]S. B. Solomon, C. Magee, D. E. Acker, and A. C. Venbrux, "TIPS placement in swine, guided by electromagnetic real-time needle tip localization displayed on previously acquired 3D CT," Cardiovasc. Intervent Radiol. **22**(5), 411–414 (1999).

[7]S. B. Solomon, P. White, Jr., D. E. Acker, J. Strandberg, and A. C. Venbrux, "Real-time bronchoscope tip localization enables three-dimensional CT image guidance for transbronchial needle aspiration in

swine," Chest **114**(5), 1405–1410 (1998).
[8]S. B. Solomon, C. A. Magee, D. E. Acker, and A. C. Venbrux, "Experimental nonfluoroscopic placement of inferior vena cava filters: use of an electromagnetic navigation system with previous CT data," J. Vasc. Interv Radiol. **10**(1), 92–95 (1999).
[9]S. C. Sporton, M. J. Earley, A. W. Nathan, and R. J. Schilling, "Electroanatomic versus fluoroscopic mapping for catheter ablation procedures: a prospective randomized study," J. Cardiovasc. Electrophysiol. **15**(3), 310–315 (2004).
[10]F. Banovac, K. Cleary, E. Levy, D. Lindisch, S. Onda, and D. Tanaka, "Design and Construction of a Liver Phantom for CT Imaging and Interventions that Simulates Liver Motion Seen During Respiration," Radiological Society of North America (RSNA), Chicago, IL, 2001, Radiol. Supl. 221, p. 689.
[11]M. Tsuchida, Y. Yamato, T. Aoki, T. Watanabe, N. Koizumi, I. Emura, and J. Hayashi, "CT-guided agar marking for localization of nonpalpable peripheral pulmonary lesions," Chest **116**(1), 139–143 (1999).
[12]K. S. Arun, T. S. Huang, and S. D. Blostein, "Least squares fitting of two 3D sets," IEEE Trans. Pattern Anal. Mach. Intell. **9**(5), 698–700 (1987).
[13]K. Cleary, F. Banovac, E. Levy, D. Tanaka, S. Onda, L. Jiang, D. Lindisch, and G. Corral, "Respiratory Liver Motion Simulator: a paradigm for percutaneous liver procedures using magnetic tracking," Computer Assisted Radiology and Surgery, Berlin, Germany, 2001.
[14]J. M. Fitzpatrick, J. B. West, and C. R. Maurer, Jr., "Predicting error in rigid-body point-based registration," IEEE Trans. Med. Imaging **17**(5), 694–702 (1998).
[15]T. de Baere, D. Elias, C. Dromain, M. G. Din, V. Kuoch, M. Ducreux, V. Boige, N. Lassau, V. Marteau, P. Lasser, and A. Roche, "Radiofrequency ablation of 100 hepatic metastases with a mean follow-up of more than 1 year," AJR, Am. J. Roentgenol. **175**(6), 1619–1625 (2000).
[16]H. Rhim and G. D. Dodd, III, "Radiofrequency thermal ablation of liver tumors," J. Clin. Ultrasound **27**(5), 221–229 (1999).
[17]G. D. Dodd, M. C. Soulen, R. A. Kane, T. Livraghi, W. R. Lees, Y. Yamashita, A. R. Gillams, O. I. Karahan, and H. Rhim, "Minimally invasive treatment of malignant hepatic tumors: at the threshold of a major breakthrough," Radiographics **20**(1), 9–27 (2000).
[18]C. H. Cha, F. T. Lee, Jr., J. M. Gurney, B. K. Markhardt, T. F. Warner, F. Kelcz, and D. M. Mahvi, "CT versus sonography for monitoring radiofrequency ablation in a porcine liver," AJR, Am. J. Roentgenol. **175**(3), 705–711 (2000).
[19]L. Solbiati, S. N. Goldberg, T. Ierace, T. Livraghi, F. Meloni, M. Dellanoce, S. Sironi, and G. S. Gazelle, "Hepatic metastases: percutaneous radio-frequency ablation with cooled- tip electrodes," Radiology **205**(2), 367–373 (1997).
[20]J. Hummel, M. Figl, C. Kollmann, H. Bergmann, and W. Birkfellner, "Evaluation of a miniature electromagnetic position tracker," Med. Phys. **29**(10), 2205–2212 (2002).
[21]T. Livraghi, S. N. Goldberg, S. Lazzaroni, F. Meloni, T. Ierace, L. Solbiati, and G. S. Gazelle, "Hepatocellular carcinoma: radio-frequency ablation of medium and large lesions," Radiology **214**(3), 761–768 (2000).
[22]L. G. Dodd, E. E. Mooney, L. J. Layfield, and R. C. Nelson, "Fine-needle aspiration of the liver and pancreas: a cytology primer for radiologists," Radiology **203**(1), 1–9 (1997).